Analysis of Resonance Stability in Power Systems with DFIG-Based Wind Generation

Luiza Buscariolli, Ahda Pavani, *Senior Member*, *IEEE* and Maurício Salles

***Abstract*-- Wind parks using doubly fed induction generators (DFIG) can interact with either series-capacitor compensated lines or weak AC grids, potentially causing instability. This paper presents a comparison of two cases that these interactions are responsible for instability. The analysis is based on Impedance-Based Stability Assessment (IBSA), which employs a frequency scanning technique to obtain the impedance profile. The generic EMT-model is use for representing the wind park. The results show different oscillations according to the power system configuration. Besides, it is also possible to highlight the oscillation cause and the different oscillation modes in both examples.**

***Index Terms*—DFIG, frequency scanning, series compensation, vector fitting, weak grids.**

I. Nomenclature

CFE – Coupling frequency effect
DFIG – Doubly Fed Inductor Generator
EMT – Electromagnetic transient
GSC – Grid-side Converter
IBSA – Impedance-based stability assessment
PI – Proportional-Integral
PLL – Phase-Locked Loop
PM – Phase Margin
POI – Point of interconnection
RSC – Rotor-side Converter
SSBSA – State-space based stability analysis
VF – Vector Fitting
WP – Wind Park

II. Introduction

WIND power generation has become one of the fastest growing electricity generation technologies, with the increasing integration of doubly fed induction generator (DFIG) based wind parks. These devices can cause major issues related to harmonics, power quality, fault ride-through capability and stability. The stability issues may lead to oscillations that are adverse to the safe operation of the grid [2]. Recent incidents have shown that the controllers of the converters can adversely interact with the series compensated lines or weakly tied AC grids [3], [4]. Therefore, there has been a growing interest in analysis, identification, and mitigation of these control interaction problems.

Events reported in different power systems are raising concerns related to the sub-synchronous resonance due to interactions of control loops of the converters employed in wind parks (WPs) with elements of the power grid [4]. References [5], [6] describe the first widely reported case of unstable subsynchronous resonance in WPs, involving DFIG generators. The WP was radially connected to a series-compensated transmission line, and circuit currents reached 4.0 pu in less than 1 second, damaging several generators and the series capacitor of the transmission line. Authors in [7], [8] report unstable resonances that led to the disconnection of large wind generation blocks. In addition to large catastrophic events, weakly damped resonances have also been reported [9]-[11]. Although quieter and more gradual, weakly damped resonance events can lead to violations of regulatory limits for harmonic distortions [12] and drastically reduce the service life of wind farm equipment.

Although DFIG usually engages in series-capacitor interactions, some researchers already demonstrated the potential instability risk of weakly-tied DFIG-WP [13] – [15]. Large wind power plants are connected to grids with relative long transmission lines. Therefore, their influence in the weak grids must be considered [16][16]. In 2018, an event was reported where an interaction between DFIG wind park and a weak grid happened, and the frequency spectrum contained 37 Hz and 63 Hz components [14].

Since the resonance involving inverters in power systems are relatively recent, although guidelines already exist, there is no consensus in the community regarding analysis methods. The analysis requires detailed models of the system and the power plants, including not only the converter and control parameters but also the analysis of operating conditions and possible grid configurations.

This paper aims to show that the interaction between DFIG-based wind parks and transmission grid with series compensation happens at the subsynchronous frequency range, while the interaction between DFIG and weak AC grids happens at supersynchronous frequency range. Considering the last, it will be demonstrated that, because the positive sequence was considered, there are inherent accuracy errors. Furthermore, because of the sharp behavior of DFIG frequency profile, the stability criteria and the vector fitting algorithm can present accuracy errors as well.

The analysis will be archived by positive sequence frequency scanning technique using single-tone injection. The Vector Fitting algorithm will be applied to calculate the eigenvalues and EMT-simulations will be made for validation. For that, the software EMTP® will be used, with MATLAB being used for post processing.

The remaining of this paper is organized as follows.

Section III briefly presents the DFIG model used in this paper, detailing the coupled frequency effect (CFE). In section IV, the main stability assessments techniques are presented. Section V and VI bring the results and conclusions, respectively.

III. DFIG Model

The topology for type III is the DFIG, with the stator of the induction generator (IG) directly connected to the grid and the wound rotor is connected to the grid through an ac-dc-ac converter system. The ac-dc-ac converter system consists of two voltage source converters (VSCs): rotor side converter (RSC) and grid side converter (GSC). A line inductor and shunt harmonic ac filters are used at the GSC to improve power quality. The rotor is fed by variable frequency currents, controlled by a converter, as seen in Fig. 1.

The generic model has two versions: detailed model (DM) and average value model (AVM). In the DM, the converters are represented by a circuit with the IGBT/diode modeled by an ideal switch and nonlinear resistors to mimic the actual behavior accurately. The AVM replicates the average response of converters through simplified functions and controlled sources, increasing the computational efficiency of the simulation. Here, the AVM model is used, reducing computational burden. More details about the modelling can be found in [18] and [34].

Due to the direct connection of the stator winding to the power grid, the DFIG-based wind power system is sensitive to the variation of the power grid, including voltage unbalance, low-voltage fault, distortions, and potential oscillations due to a comparatively large impedance of the weak grid which is large enough to be neglected and requires attention [17].

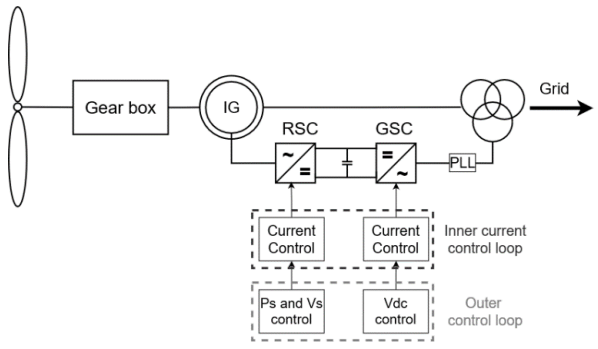

Fig. 1. Scheme of the structure of the DFIG with its controllers.

In this work, the implemented control strategy is the grid-following type, represented by their average model. In both rotor-side and grid-side converters, a cascade control scheme is considered, consisting of an external control loop and an internal control loop. More details about control and operation can be found in [18].

The phase locked loop (PLL) is the element used to synchronize the control system with the grid, maintaining the phase and frequency between two signals and continuously applying the Park transformation. The PLL is responsible for the coupling frequency effect (CFE), also called mirror frequency effect. CFE refers to the phenomenon that a coupling voltage/current component appears along with the dominant voltage/current component at resonance frequency. As explained in [13] and [19], the CFE arises due to the asymmetry in inverter-based model caused by the PLL and different outer-loop control strategies in *d*- and *q*- axis. Basically, because K_d and K_q are not equal, when transforming an AC quantity from abc reference frame to *dq* reference frame and then back to abc, a frequency component appears that fulfills a mirror symmetry relationship. This can be seen in equation (1), where f_{NOM} is the nominal frequency, f_r is the resonant frequency, and f_{CFE} is the coupled frequency.

$$|f_{CFE}| = |2f_{NOM} - f_r| \quad (1)$$

Wind turbine suppliers do not disclose many details of the internal control circuitry [19]. However, they provide black-box models of the generators. Alternatively, it is possible to use generic EMT models of wind turbines. These models are standardized, publicly available, and capable of capturing all aspects of performance as effectively as manufacturer-specific models [19], [20]. These models have been validated by comparing the results with different field experiments and have been used as an alternative for resonance studies when the black-box model of the generator provided by the manufacturer is not available.

In the simulations, the aggregated model of the WP is used, which provides a reasonable approximation for system interconnection studies [21],[22].

IV. Proposed Method

Electromagnetic transient (EMT) simulations are used as a first approach to illustrate resonance in power systems. The EMT method can simulate nonlinear and switching devices without simplifications, also considering extremely short time constants. This ensures the accuracy and efficiency of the studies. Even when other techniques are used to identify critical conditions, it is common for critical conditions to be validated with EMT simulations [23][23], [24].

A. Impedance-Based Stability Assessment

The impedance-based stability assessment (IBSA) has been standing out to evaluate the stability, especially when only the EMT-black box model is available. In this case, the frequency scanning technique is used to calculate the equivalent impedance measured at the POI [26]. The evaluation of the system impedance for a range of frequencies is a widely used measure to describe the linearized characteristics of an electrical system [26]. This method assesses the risk of resonance using simulation data or measurement data. It represents a solution to address the restrictions imposed by the usage of black-box models. However, this method alone does not provide information about the system oscillation modes and their damping, which are generally required to support mitigation studies [27]. Fig. 2 represents the frequency scanning to the WP-side using current disturbance.

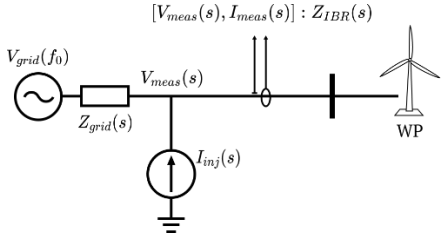

Fig 2. WP side frequency scan using current disturbance

The properties of the imposed signal, such as frequency, shape and amplitude, are parameters of the procedure. Abrupt disturbances can trigger nonlinearities in some cases. The disturbance amplitude should be as high as possible, but it cannot excite nonlinearities and saturation effects [2]. The range of studied frequencies can be introduced all at once (multi tone disturbance), or they can be introduced one by one (single-tone disturbance). The literature shows that single tone disturbance brings more accurate results although the simulation takes longer.

1) Stability Criteria

Once the impedances have been obtained, stability criteria can be used, as magnitude and phase angle rules (Bode plots), reactance crossover criterion (R-X plots) and/or Nyquist criterion (Nyquist diagram). The R-X criterion is straightforward. For this criterion, the total system impedance, consisting of the grid and wind farm impedance ($Z_{sys}(f) = Z_{grid}(f)+Z_{WP}(f)$), is calculated, and its resistance (R_{sys}) and reactance (X_{sys}) are plotted separately. Resonance is determined according to the rule in (3), where f_i is a frequency within a frequency range of interest [28].

$$R_{sys}(f_i)\left(\frac{dX_{sys}(f_i)}{df_i}\right)|_{f_i=f_c} < 0 \qquad (3)$$

Any reactance zero-crossover from negative to positive that coincides with a negative resistance indicates an unstable resonance at the given frequency [30]. The negative resistance is the responsible for the lack of damping, and therefore, the unstable resonance.

Although the easy visualization and fast evaluation, the R-X plots cannot show the phase margin, only the resonant frequency. One way to overcome this is use the Bode plot. The potential control interactions are initially located at the intersection points of magnitude curves of WP and grid impedances. Instabilities are then determined by the phase angle difference between the grid and WP impedances. A positive phase margin means the system is stable, while a negative phase margin means it's unstable. The larger the positive phase margin, the more stable the system is.

B. State-Space Based Stability Analysis

For conventional power systems, the modal analysis is performed by state-space based stability analysis (SSBSA). The advantage of this approach is that through eigenvalues, it is possible to observe the oscillatory modes, as well as the damping of the oscillation modes. Eigenvalues are complex numbers, as seen in (2). The real part (σ) corresponds to the damping and the imaginary part (ω) brings information about the frequency.

$$\lambda = \sigma \pm j * \omega \qquad (2)$$

If the real part is positive, the mode is unstable, and the angular frequency corresponds to the frequency of the oscillation. Furthermore, with this approach it is possible to calculate the participation factors, from which it is possible to observe the impact of each variable. An additional advantage of eigenvalues is that when several scenarios are studied, it is possible to observe the behavior of the eigenvalues, showing whether different scenarios make the system more prone to instability.

However, a major disadvantage of this method is that it requires a detailed mathematical representation of the system to obtain its state space, which may not be available, since it is common for wind turbine manufacturers to provide black-box models for EMT-type simulations, due to intellectual property concerns. Even with complete models, the state space equations often require lengthy calculations due to the complex controllers. These controllers are not standardized and the equations for each case need to be re-evaluated when one or more parameters change [25]. Table I summarizes the main advantages and disadvantages of the methods considered.

C. Vector Fitting

A solution to obtain the eigenvalues from frequency scanning results is to apply a fitting algorithm to estimate the system's eigenvalues. The Vector Fitting (VF) algorithm [29]-[31] approximates a frequency response Z(s) (generally a vector) with a rational function, expressed in the form of a sum of partial fractions based on the pole-residue representation, which can be represented as in (4), where r_i is the residue corresponding to the eigenvalue λ_i, and D and E are optional parameters. Note that the eigenvalue in (4) is represented in the same way as in (2), bringing the same information. The computational routine is public available online using MATLAB [32].

$$Z(s) = \sum_{i=1}^{n} \frac{r_i}{s-\lambda_i} + D + sE \qquad (4)$$

The fit order must be as small as possible, minimizing the error between the algorithm's response and the measured frequency behavior. Considering a black-box approach, the number of states (or the fit order (n)) in the system is unknown. Moreover, the resulting eigenvalues cannot be related to any physical quantities in the system. This is a consequence of having a black-box approach in general, and not a weakness of the method. To adjust the fit order, a methodology is presented in [33] to identify insignificant states and eigenvalues. When the ratio of the residue r_i by the eigenvalue λ_i has small absolute value for the state i, this state does not contribute to the measured response.

TABLE I
COMPARISON OF SSI ANALYSIS TECHNIQUES

METHOD	ADVANTAGES	DISADVANTAGES
EMT	• It can simulate nonlinear and switching devices without simplifications. • Amplitude of the oscillations can be observed. • Most accurate method.	• Complete model is expensive. • Complicated for large systems • Multiple simulations are time consuming.
SSBSA	• Information about frequency and damping for each mode. • Explicit internal relationships between variables. • Helpful for mitigation measures design.	• It cannot be used with black-box models. • State-space equations require long calculations • Definition of the linearization point. • For any change in the system, all calculation must be redone.
IBSA	• Fast estimation of resonance risk. • It can be used with black-box models. • It can be done for different contingencies.	• It does not provide information about damping. • inappropriate parameters leading to poor results.

It is important to mention that as the impedance is obtained via frequency scanning, the value of the apparent impedance (Z_{app}) shall be used as input to the Vector Fitting algorithm, once the definition of the apparent impedance assumes an injection of voltage or current at some point in the power system.

Fig. 3 shows the flowchart of the proposed method.

Fig. 3 – Flowchart of the proposed method

V. RESULTS

Fig. 4 shows the scheme of the test system for the study of the interaction between DFIG WPs, and series compensated networks or weak grids. The WP is connected to the system though two parallel transmission lines, one line connected to the Network 1 and one transmission line connected to Network 2. Two different configurations are assumed for Network 1. The first one, Case 1, the transmission line is series compensated. In the second one, Case 2, the transmission line is connected to a weak grid.

The simulation has 5 s. At t = 2 s, a fault happens on line 2 and at t= 2.1 s the breaker opens, resulting in the WP connected to the grid only through Network 1, representing the two studied cases. For Case 1, the wind speed is kept at 7 m/s and the series capacitor banks, X_C, connected at both terminals of line 1 are employed for a variable level of series compensation. Two scenarios were considered, S1 and S2, with 40% and 55% of compensation, respectively. For case 2, the wind speed is 5 m/s and the value short-circuit impedance, Z_{G1}, is changed to represent a weak grid. Two scenarios were considered, first a strong grid, with SCR = 5, and the second, a weaker grid, with SCR = 2.5.

For both cases the values were selected to better present the results, showing damped and undamped oscillations, respectively. The scenarios are summarized in Table II. Table III shows the main parameters of the simulations The remaining parameters are presented in Tables IV and V in the Appendix.

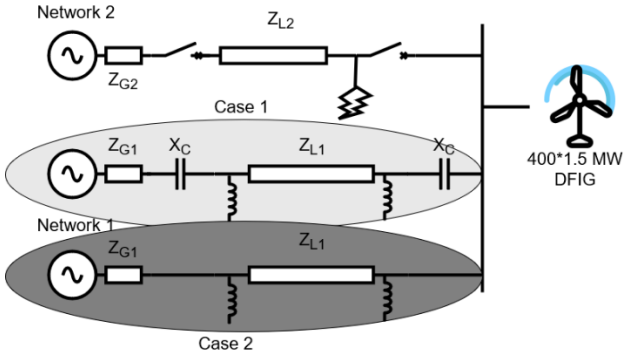

Fig. 4 – Circuit of the test system.

TABLE II
SIMULATION SCENARIOS

CASE 1 (V = 7M/S)	S1	35 % compensation level
	S2	45 % compensation level
CASE 2 (V = 5M/S)	S3	Strong Grid (SCR = 5)
	S4	Weak Grid (SCR = 2.5)

TABLE III
SIMULATION PARAMETERS

PARAMETER	VALUE
System frequency	60 Hz
Power base	666.8 MVA
Voltage base	500 kV
Wind Speed	Case 1: 7 m/s Case 2: 5m/s
Shunt compensation	68.8 %

To characterize the interactions observed in the WP, simulations were performed in the time domain, as well as frequency scanning, using the EMTP software. MATLAB was used to process the data. The scan of WP and grid was performed separately. WP scan was performed as seen in Fig. 2. The grid side impedance is obtained using the phasor solution-based impedance scanning tool.

A. Series compensation interaction (Case 1)

With the compensation level at 40%, it is observed that, after the circuit breakers are opened, a small 23 Hz component appears in the WP current, as seen in Fig. 5. In Fig. 6, the impedance curve crosses the zero three times. Only the first and third points fulfill the criterion on (2). The first point has a clearly positive resistance. For the third point, it is possible to observe that near f = 23 Hz the resistance value is low but still positive, indicating a stable scenario. As an alternative way to

observe the results, the Bode plot is brought in Fig. 7. Applying the magnitude and phase angle rules, the grid impedance is equal to that of the WP in 2 points and at f = 23 Hz the phase margin (PM) is small but positive and it is equals to 4.8°.

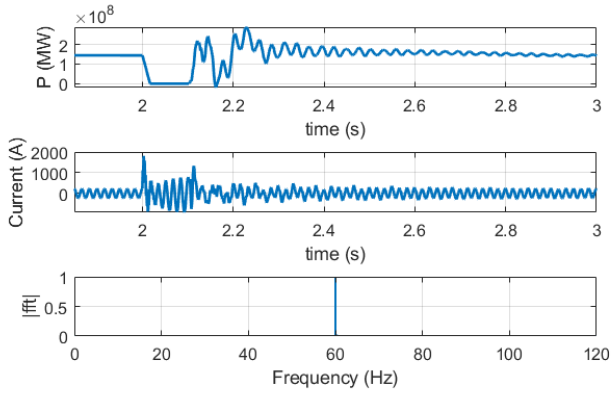

Fig. 5 – EMT simulation for case 1 S1 (V = 7m/s and X_C = 40%)

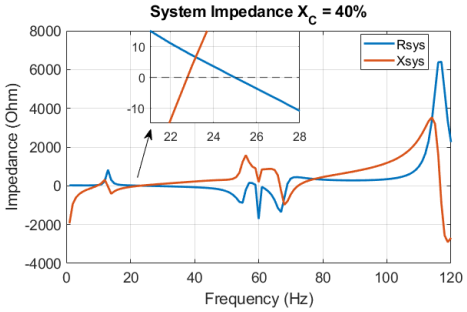

Fig. 6 – R-X plot for case 1 S1 (V = 7m/s and X_C = 40%)

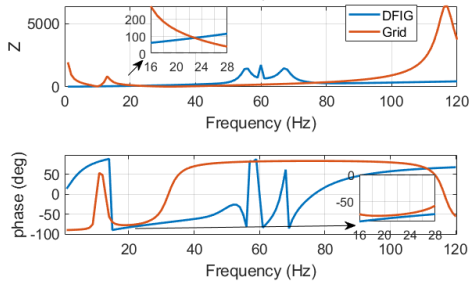

Fig. 7 – Bode plot for case 1 S1

Once the frequency response is obtained, the VF is performed. The suitable fitting order was selected at N = 10 and knowing that the interaction happens at a subsynchronous frequency, the VF was applied to a portion of the frequency scanning profile, from 1 Hz to 50 Hz. This reduces the fitting order. The VF routine has the option to enforce stable poles, which was selected, since stability criteria of the impedance technique was reached. Fig. 8 shows the behavior of the eigenvalues for the scenario S1. As one can see, all eigenvalues are negative indicating a stable condition.

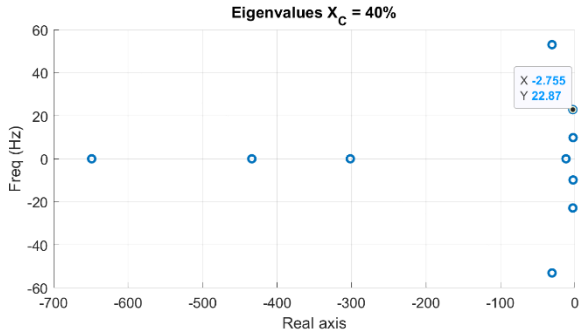

Fig. 8 – Eigenvalues for case 1 S1 (rms = 1.92)

With the compensation level at 55% in scenario S2, it is observed in Fig. 9 that, after the circuit breakers are opened, a 27 Hz component appears in the WP current together with a small 93 Hz component, evidencing the CFE. However, the unstable oscillation mode is associate to 27 Hz frequency, which can be verified by the impedance curve as follows.

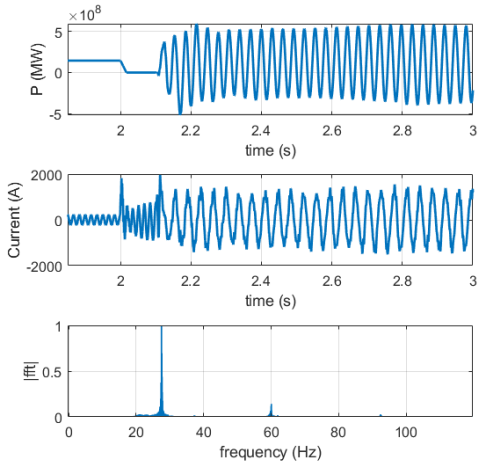

Fig. 9 – EMT simulation for case 1 S2 (V = 7m/s and X_C = 55%)

Fig. 10 shows the impedance curve, the imaginary part of the impedance crosses the zero three times. Only the first and third points fulfill the criterion on (2). The first point has a clearly positive resistance. It is possible to observe that near f = 27 Hz the resistance value is negative, indicating an unstable scenario. For the Bode plot in Fig. 11, the grid impedance is equal to that of the WP in 2 points and at f = 27 Hz the phase margin is negative, and it is equals to -1.5°.

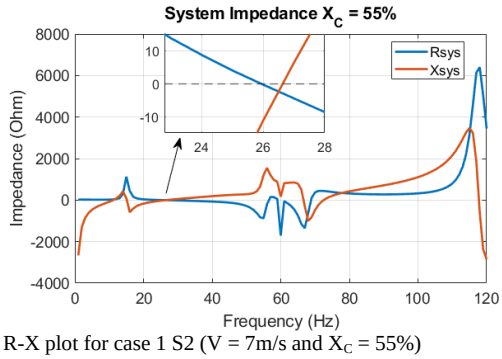

Fig. 10 – R-X plot for case 1 S2 (V = 7m/s and X_C = 55%)

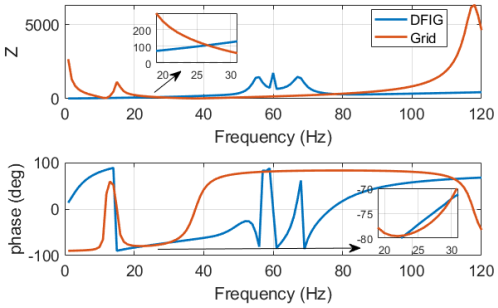

Fig. 11 – Bode plot for case 1 S2 (V = 7m/s and X_C = 55%)

Once the frequency response is obtained, the VF is performed. This time, the poles could be unstable, and the fitting order was kept at N = 10. Fig. 12 shows the behavior of the eigenvalues for the scenario S2. There are two eigenvalues in the Right-Half Plane indicating an unstable condition. One of these eigenvalues is located around f = 26.6 Hz, indicating that this is a resonant frequency that leads the system to the instability. It is important to remember that the eigenvalues calculated with VF have no physical meaning.

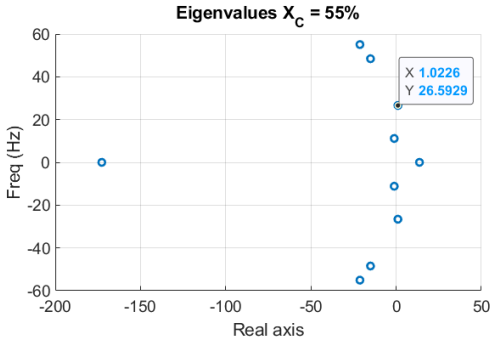

Fig. 12 – Eigenvalues for case 1 S2 (rms = 2.38)

B. *Weak grid interaction (Case 2)*

This case was simulated using the parameters shown in Table V. Considering a strong grid, with SCR = 5, it possible to observe in Fig. 13 that, after the breaker opens, the system returns to a stable operation point. The impedance plot of the system is presented in Fig. 14. As one can see, the reactance becomes positive around f = 72 Hz. At this point, the resistance has a positive value, characterizing the system stability.

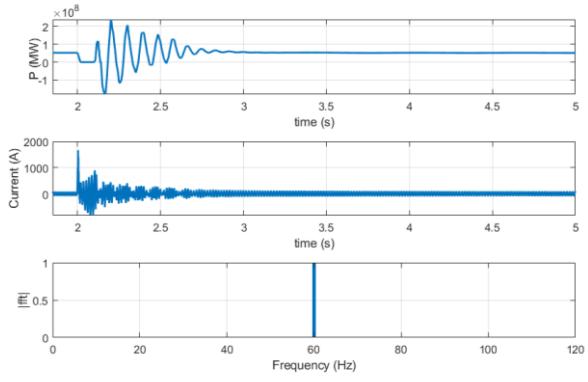

Fig 13 – EMT simulation for case 2 S3 (Strong Grid)

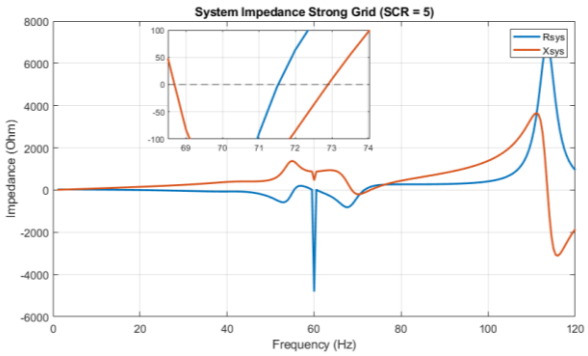

Fig. 14 – R-X plot for Strong Grid

The Bode plot in Fig. 15 shows that around 73 Hz the impedances of DFIG wind park and the grid are equal and at f = 71.5 Hz the PM=-1.12°. As the DFIG phase angle has a sharp behavior, it may indicate that the region around 70 Hz is a dangerous region, since the PM can vary very fast for small frequency steps. Since the frequency where the impedances are equal are different from the frequency where the PM <0, it indicates a stable scenario.

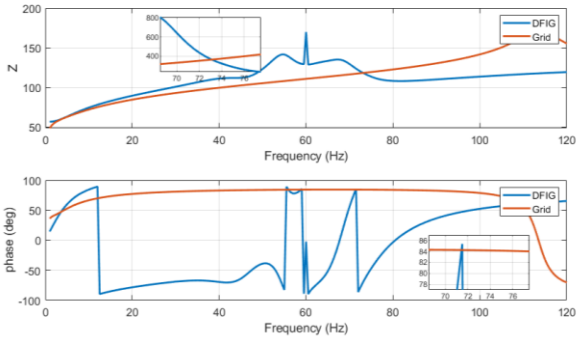

Fig. 15 – Bode plot for scenario S3 Strong Grid

Once the frequency response is obtained, the VF is performed. The suitable fitting order was kept at N = 10, Knowing that the interaction happens near the nominal frequency, the VF was applied to a portion of the frequency scanning profile, from 40 Hz to 80 Hz. This helps reducing the fitting order. The VF routine has the option to enforce stable poles, which was selected. Fig. 16 shows the behavior of the eigenvalues for the scenario S3. As can be noticed, the eigenvalues are all negative.

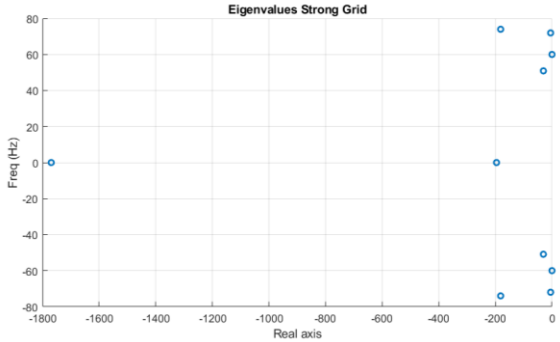

Fig. 16 – Eigenvalues for scenario S3 (rms = 3.1)

The Scenario 4 is simulated, considering a weak grid, with SCR = 2.5. In the time simulation, after the breaker opens, it possible to observe that two components appear at the WP current, one at 70 Hz and another at 50 Hz, as can be seen in Fig. 17.

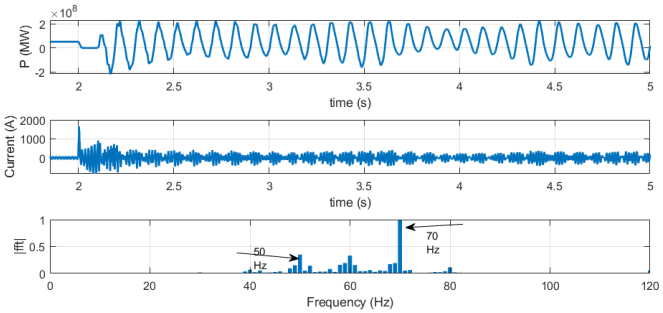

Fig. 17 – EMT simulation for scenario S4: weak grid

Fig. 18 shows that the reactance becomes positive around f = 70.5 Hz. At this point, the resistance has a negative value, indicating an unstable scenario.

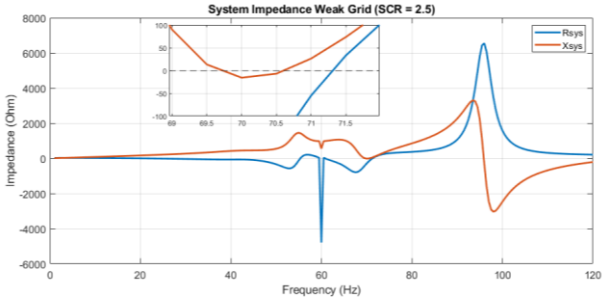

Fig. 18 – R-X plot for Weak Grid

The Bode plot in Fig. 19 shows that around 71 Hz the impedances of DFIG wind park and the grid are equal and PM = -2.79°. Again, the sharp behavior is observed. It translates into a phase margin that can become positive for a small frequency step. Although the instability is detected, it does not hit the exact frequency that the oscillation happens. It might indicate an accuracy issue in the FFT window and/or in the frequency scan procedure.

The VF is performed. The fitting order was kept at N = 10. Fig. 20 shows the behavior of the eigenvalues for the scenario S4. It possible to observe that the eigenvalues around f = 50 Hz are stable, while the poles around f = 70 Hz are unstable. Although the eigenvalues do not have a physical meaning, it is a strong indication that the weak grid interaction is, in fact, supersynchronous.

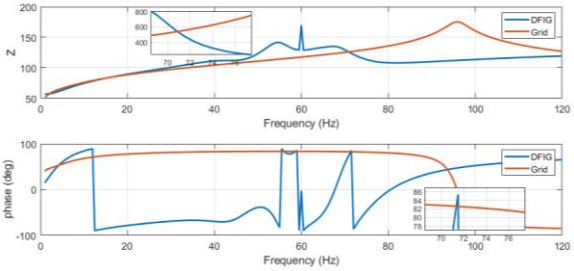

Fig. 19 – Bode plot for scenario S4 Weak Grid

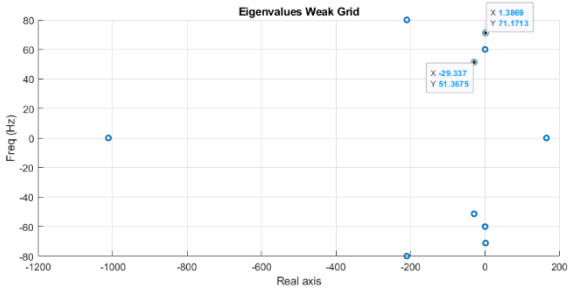

Fig. 20 – Eigenvalues for scenario S4 (rms = 1.0532)

VI. Conclusion

Wind parks with DFIG can interact with both series-capacitor compensated and weak AC grids, thus causing instability.
Considering the positive sequence frequency scanning, three stability criteria were used to define if the interactions were sub or supersynchronous: RX-plot, Bode plot and VF. Because of the sharp behavior of DFIG frequency profile, the stability criteria considered, and the VF algorithm presented accuracy issues when assessing the interaction between DFIG and weak grids. Therefore, further studies on the interaction between DFIG-WP and weak grids are needed. The stability criteria are, so far, suitable for studies of interaction between DFIG and series compensation that happens at subsynchronous range, where the DFIG behavior is smother.
Interaction between DFIG and series compensation is subsynchronous and is affected by the compensation level.
Interaction between DFIG and weak grid is supersynchronous and is affected by the PLL and GSC parameters.

VII. Appendix

Remaining parameters can be obtained at [2], [13] and [14]

TABLE IV
Simulation Parameters – Transmission Line

Parameter	Value
Rated Voltage	500 kV_{RMS-LL}
Line Length of Line 2	100 km
Line Length of Line 1	500 km
R_0 (Transmission Line)	0.0283 Ω/km
X_{L0} (Transmission Line)	0.3244 Ω/km
Charging capacitance G_{C0}	5.0512 µS/km
Equivalent impedance of System-1 (ZG1)	Case 1 and Case 2 (Strong grid): 7.5+j75 Ω Case 2 (weak grid): 15+j150 Ω
Equivalent impedance of System-2 (ZN2)	5+j75 Ω

TABLE V
Simulation Parameters – Wind Park

Parameter	Value
Rated power of wind turbines	1.667 MVA
Wind turbine rated power	1.5 MW
Rated Voltage of WT	0.575 kV_{RMS-LL}
DFIG GSC inner loop rise time	10 ms

DFIG RSC inner loop rise time	Case 1 – 20 ms Case 2 – 18 ms
Kp PLL	Case 1 – 33 Case 2 – 55
Ki PLL	Case 1 – 100 Case 2 – 200

VIII. Acknowledgment

The authors gratefully acknowledge the support of the RCGI – Research Centre for Greenhouse Gas Innovation (23.1.8493.1.9), hosted by the University of São Paulo (USP), sponsored by FAPESP – São Paulo Research Foundation (2020/15230-5), and sponsored by TotalEnergies, and the strategic importance of the support given by ANP (Brazil's National Oil, Natural Gas and Biofuels Agency) through the R\&DI levy regulation.

IX. References

[1] Empresa de Pesquisa Energética – EPE. Brazilian Energy Balance 2023 Year 2022. Rio de Janeiro: EPE, 2023. [Online]. Available: https://www.epe.gov.br/sites-pt/publicacoes-dados-abertos/publicacoes/PublicacoesArquivos/publicacao-748/topico-687/BEN2023.pdf

[2] K. Jacobs, Y. Seyedi, L. Meng, U. Karaagac and J. Mahseredjian. "A comparative study on frequency scanning techniques for stability assessment in power systems incorporating wind parks." *Electric Power Systems Research*, vol. 220, 2023. https://doi.org/10.1016/j.epsr.2023.109311.

[3] Y. Cheng et al., "Real-World Subsynchronous Oscillation Events in Power Grids with High Penetrations of Inverter-Based Resources," *IEEE Trans. Power Syst*., vol. 38, no. 1, pp. 316-330, Jan. 2023.

[4] IEEE-PES Wind SSO Task Force, "Wind energy systems sub-synchronous: events and modeling," Technical Report, PES-TR80, AMPS oscillations Committee, 2020.

[5] G. D. Irwin, A. K. Jindal, and A. L. Isaacs, "Sub-Synchronous Control Interactions between Type 3 Wind Turbines and Series Compensated AC Transmission Systems," in *Proc. IEEE PES General Meeting*, pp. 1-6, 2011.

[6] D. Kidd and P. Hassink, "Transmission Operator Perspective of Sub-Synchronous Interaction," in *Proc. IEEE PES Transmission & Distribution*, pp. 1-3, 2012.

[7] X. Xie, X. Zhang, H. Liu, H. Liu, Y. Li, and C. Zhang, "Characteristic Analysis of Subsynchronous Resonance in Practical Wind Farms Connected to Series-Compensated Transmissions," *IEEE Transactions on Energy Conversion*, vol. 32, no. 3, pp. 1117-1126, 2017.

[8] H. Liu, X. Xie, J. He, T. Xu, Z. Yu, C. Wang, and C. Zhang, "Subsynchronous Interaction Between Direct-Drive PMSG Based Wind Farms and Weak AC Networks," *IEEE Transactions on Power Systems*, vol. 32, no. 6, pp. 4708-4720, 2017.

[9] C. Larose, R. Gagnon, P. Prud'Homme, M. Fecteau, and M. Asmine, "Type-III Wind Power Plant Harmonic Emissions: Field Measurements and Aggregation Guidelines for Adequate Representation of Harmonics," *IEEE Transactions on Sustainable Energy*, vol. 4, no. 3, pp. 797- 804, 2013.

[10] Z. Liu, J. Rong, G. Zhao, and Y. Luo, "Harmonic Assessment for Wind Parks Based on Sensitivity Analysis," *IEEE Transactions on Sustainable Energy*, vol. 8, no. 4, pp. 1373-1382, 2017.

[11] K. Yang, M. H. J. Bollen, and E. O. A. Larsson, "Aggregation and Amplification of Wind Turbine Harmonic Emission in a Wind Park," *IEEE Transactions on Power Delivery*, vol. 30, no. 2, pp. 791-799, 2015.

[12] National System Operator (ONS), "Gerenciamento dos indicadores de desempenho da rede básica e de seus componentes," PROREDE – Submódulo 2.8 (Brazilian regulation), 2008. Online. Available: https://www.ons.org.br/%2FProcedimentosDeRede%2FM%C3%B3dulo%202%2FSubm%C3%B3dulo%202.8%2FSubm%C3%B3dulo%202.8_Rev_0.3.pdf (in Portuguese).

[13] M. Lei. EMT-type impedance scanning methods for screening control interactions between inverter-based resource and transmission grid. PhD thesis. Department of Electrical and Electronic Engineering, The Hong Kong Polytechnic University. 2024.

[14] T. Xue, U. Karaagac, L. Cai and I. Kocar, "Re-Examination of DFIG-Based Wind Park Small-Signal Instability," in IEEE Access, vol. 11, pp. 141740-141752, 2023, doi: 10.1109/ACCESS.2023.3340703.

[15] L. Fan, Z. Miao, Analytical model building for Type-3 wind farm subsynchronous oscillation analysis, Electric Power Systems Research, V. 201, 2021, https://doi.org/10.1016/j.epsr.2021.107566

[16] L. -J. Cai and I. Erlich, "Doubly Fed Induction Generator Controller Design for the Stable Operation in Weak Grids," in *IEEE Transactions on Sustainable Energy*, vol. 6, no. 3, pp. 1078-1084, July 2015, doi: 10.1109/TSTE.2014.2338492.

[17] Y. Song and F. Blaabjerg, "Overview of DFIG-Based Wind Power System Resonances Under Weak Networks," in *IEEE Transactions on Power Electronics*, vol. 32, no. 6, pp. 4370-4394, June 2017. 10.1109/TPEL.2016.2601643.

[18] U. Karaagac et al. Simulation Models for Wind Parks with Variable Speed Wind Turbines in EMTP. 2017. [Online]. Available: https://www.emtp.com/documents/EMTP%20Documentation/doc/advanced/WP_documentation.pdf

[19] W. Ren and E. Larsen, "A Refined Frequency Scan Approach to Sub-Synchronous Control Interaction (SSCI) Study of Wind Farms," *IEEE Transactions on Power Systems*, vol. 31, no. 5, pp. 3904-3912, 2016.

[20] A. Haddadi, I. Kocar, T. Kauffmann, U. Karaagac, E. Farantatos and J. Mahseredjian, "Field validation of generic wind park models using fault records," in *Journal of Modern Power Systems and Clean Energy*, vol. 7, no. 4, pp. 826-836, July 2019, doi: 10.1007/s40565-019-0521-x

[21] L. Fan, R. Kavasseri, Z. L. Miao, and C. Zhu, "Modeling of DFIG-based wind farms for SSR analysis," *IEEE Transactions on Power Delivery*, vol. 25, no. 4, pp. 2073–2082, Oct. 2010, doi: 10.1109/TPWRD.2010.2050912.

[22] H. Liu, X. Xie, C. Zhang, Y. Li, H. Liu and Y. Hu, "Quantitative SSR Analysis of Series-Compensated DFIG-Based Wind Farms Using Aggregated RLC Circuit Model," in *IEEE Transactions on Power Systems*, vol. 32, no. 1, pp. 474-483, Jan. 2017, doi: 10.1109/TPWRS.2016.2558840.

[23] A. M. A. Elgaali, "Sub-synchronous controller interaction (SSCI) of series-compensated DFIG wind farms" master's Dissertation, Dept. of Energy and Environment, Chalmers Univ. of Technology Gothenburg, Sweden 2016.

[24] R. N. Damas, Y. Son, M. Yoon, S. -Y. Kim and S. Choi, "Subsynchronous Oscillation and Advanced Analysis: A Review," *in IEEE Access*, vol. 8, pp. 224020-224032, 2020, doi: 10.1109/ACCESS.2020.3044634.

[25] Shirinzad, M. Frequency Scan Based Stability Analysis of Power Electronic Systems. Thesis (master's in science) – Faculty of Graduate Studies of The University of Manitoba. Manitoba, 2021.

[26] B. Badrzadeh, M. Sahni, Y. Zhou, D. Muthumuni and A. Gole, "General Methodology for Analysis of Sub-Synchronous Interaction in Wind Power Plants," in *IEEE Transactions on Power Systems*, vol. 28, no. 2, pp. 1858-1869, May 2013, doi: 10.1109/TPWRS.2012.2225850.

[27] A. S. Trevisan, M. Fecteau, A. Mendonça, R. Gagnon, J. Mahseredjian, Analysis of low frequency interactions of DFIG wind turbine systems in series compensated grids, Electric Power Systems Research, Volume 191, 2021, 106845, ISSN 0378-7796, https://doi.org/10.1016/j.epsr.2020.106845.

[28] Alatar, F.; Mehrizi-Sani, A. "Frequency Scan–Based Mitigation Approach of Subsynchronous Control Interaction in Type-3 Wind Turbines," *Energies*, vol. 14, pp. 4626-. https://doi.org/10.3390/en14154626

[29] B.Gustavsen and A. Semlyen, "Rational approximation of frequency domain responses by Vector Fitting", *IEEE Trans. Power Delivery*, vol. 14, no. 3, pp. 1052 - 1061, July 1999.

[30] B. Gustavsen, "Improving the pole relocating properties of vector fitting", *IEEE Trans.Power Delivery*, vol 21, no 3, pp 1587-1592, July 2006

[31] D. Deschrijver, M. Mrozowski, T. Dhaene and D. de Zutter: "Macromodeling of Multiport Systems Using a Fast Implementation of the Vector Fitting Method", *IEEE Microwave and Wireless Components Letters*, vol. 18, no 6, pp 383-385, June 2008

[32] B. Gustavsen. Vector Fitting. Online. Available: https://www.sintef.no/en/software/vector-fitting/

[33] A. Rygg and M. Molinas, "Apparent Impedance Analysis: A Small-Signal Method for Stability Analysis of Power Electronic-Based Systems," in *IEEE Journal of Emerging and Selected Topics in Power Electronics*, vol. 5, no. 4, pp. 1474-1486, Dec. 2017, doi: 10.1109/JESTPE.2017.2729596

[34] T. Kauffmann, U. Karaagac, I. Kocar, S. Jensen, J. Mahseredjian and E. Farantatos, "An Accurate Type III Wind Turbine Generator Short Circuit Model for Protection Applications," in *IEEE Transactions on Power Delivery*, vol. 32, no. 6, pp. 2370-2379, Dec. 2017, doi: 10.1109/TPWRD.2016.2614620.

X. BIOGRAPHIES

Luiza Buscariolli holds a degree in Energy Engineering (2019) and a master's degree in Energy (2022) from the Federal University of ABC (UFABC). She is currently a PhD student in Energy at the same institution, researching resonance in wind farms.

Ahda P. Grilo Pavani (Senior Member, IEEE) is currently an associate professor at the Federal University of ABC (UFABC). She holds PhD in Electrical Engineering from the State University of Campinas (UNICAMP) (2008). She completed her postdoctoral at UNICAMP with an internship at the University of Alberta, Canada. She is a member of the IEEE Power System Dynamic Performance Committee, being TCPC of the committee from 2019 to 2021, and is currently the secretary of the Working Group on Dynamic Performance of Renewable Energy Systems of the PSDP Committee. She is an associate editor of the Journal of Control Automation and Electrical Systems and IEEE Transactions on Sustainable Energy.

Maurício Barbosa de Camargo Salles is an associate professor at the Polytechnic School, USP, since 2010. From 2006 to 2008, he joined the research team of the Institute of Electrical Machines, RWTH Aachen University. Between 2014 and 2015, he was a Visiting Scholar at Harvard John A. Paulson School of Engineering and Applied Sciences. His main research interests include distributed generation, power system dynamics, control and stability, renewable energy, energy storage, and electricity markets